



e-ISSN: 2319-8753 | p-ISSN: 2347-6710

# IJRSET

International Journal of Innovative Research in  
**SCIENCE | ENGINEERING | TECHNOLOGY**

# INTERNATIONAL JOURNAL OF INNOVATIVE RESEARCH

IN SCIENCE | ENGINEERING | TECHNOLOGY

Volume 12, Issue 4, April 2023

**ISSN** INTERNATIONAL  
STANDARD  
SERIAL  
NUMBER  
INDIA

Impact Factor: 8.423

9940 572 462

6381 907 438

[ijirset@gmail.com](mailto:ijirset@gmail.com)

[www.ijirset.com](http://www.ijirset.com)



# Photovoltaic-Wind and Hybrid Energy Storage Integrated Multi-Source Converter Configuration for DC Microgrid Applications

Y. Rajesh Babu, G Narayana Sai Ganesh, Sk Tousif Riyaz, K Kiran, T.Niranjan Raju,

P Venu Madhav

Assistant Professor, Department of Electrical and Electronics Engineering, KKR & KSR Institute of Technology and Sciences, Guntur, A.P., India

Department of Electrical and Electronics Engineering, KKR & KSR Institute of Technology and Sciences, Guntur, A.P., India

Department of Electrical and Electronics Engineering, KKR & KSR Institute of Technology and Sciences, Guntur, A.P., India

Department of Electrical and Electronics Engineering, KKR & KSR Institute of Technology and Sciences, Guntur, A.P., India

Department of Electrical and Electronics Engineering, KKR & KSR Institute of Technology and Sciences, Guntur, A.P., India

**ABSTRACT:** In this paper, a new multi-source and Hybrid Energy Storage (HES) integrated converter configuration for DC microgrid applications is proposed. Unlike most of the multi-input converter configurations, a supercapacitor-battery based HES is interfaced which effectively handle the power fluctuations due to the wind, photovoltaic and sudden load disturbances. Integration of supercapacitor to respond for high- frequency fluctuations increase the lifetime of battery storage and reduce the sizing of the storage unit. The control structure is framed to achieve power balance in the system along with basic functionality such as operating renewable sources (PV and wind) at maximum power point and charging and discharging of energy storage based on power availability. The key highlights of the proposed configuration are:

- i. Less number of switches,
- ii. Voltage boosting, voltage regulation of supercapacitor and power-sharing among battery and supercapacitor are inherent,
- iii. Simple control structure with a reduced number of sensors. The detailed analysis, modeling, and design of the proposed configuration and control structure are presented along with MATLAB simulations and experimental validations.

**KEYWORDS:** Battery, DC microgrid, Hybrid Energy Storage (HES), Multi-port converter, Photovoltaic, Supercapacitor and Wind.

## I. INTRODUCTION

Renewable A energy sources such as Photovoltaic (PV) and wind are the dominant part of total renewable power generation. Since, both the sources are intermittent in nature, effective solutions are needed for reliable operation. The inherent advantage of PV and wind is that they are complement in nature. Hence, the combination of PV and wind sources can address the problem of long term intermittency to some extent. But, because of this, the severity of short term power fluctuations will be more which leads to high stress on battery storage and sizing of the battery may increase. Moreover, lifetime of the battery gets affected. Hence, by combining battery and supercapacitor as a hybrid energy storage, the problem of battery lifetime degradation and increased sizing can be addressed. Moreover, since the

voltage rating of PV, wind, and storage units are usually less, boosting of voltages is also needed. Therefore, a suitable converter configurations and control structures for the integration of Hybrid Energy Storage and renewable power sources are the major research areas. Appreciable research has been done and reported in literature regarding the interfacing configurations of battery supercapacitor based HES and renewable power sources. Various HES interfacing configurations reported in literature are shown in Fig.1.

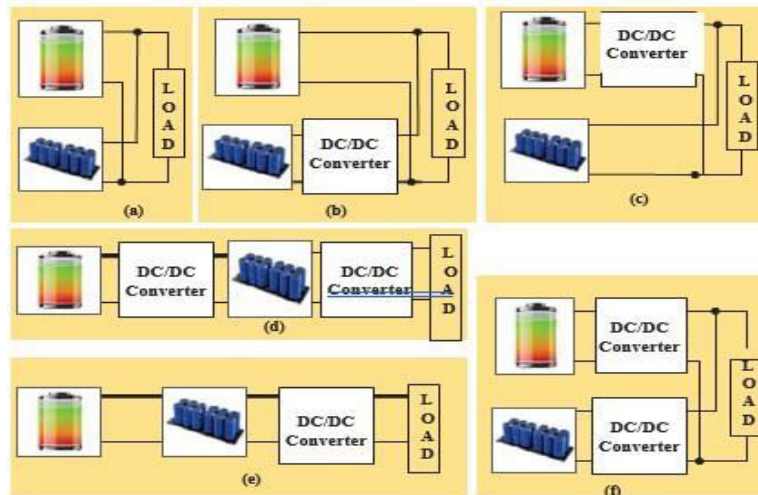


Fig. 1. Various hybrid energy storage converter configurations

The configuration shown in Fig. 1(a) is a passive connection of HES. Where, both the battery and supercapacitor has been connected directly to the load. Though low cost and simple connection being the advantages, poor volumetric efficiency and absence of transient power sharing are the drawbacks of this configuration. Moreover, the voltage rating of battery and supercapacitor should match with the voltage rating of dc-link which affects sizing of HES

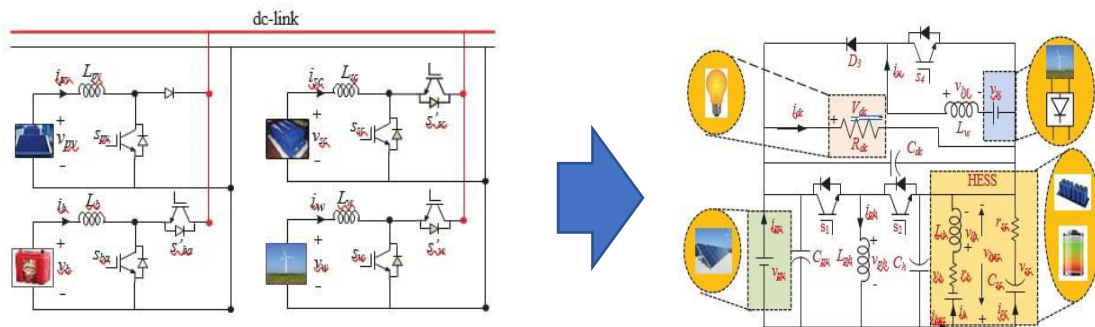


Fig. 2. Typical DC microgrid configuration Fig. 3. Proposed multi-source converter configuration

The configurations shown Fig. 1(b) and Fig. 1(c) are the semi-active configurations. In these configurations, either battery or supercapacitor has been connected to the load via a dc-dc converter. With these configurations, the drawbacks of passive connection in Fig. 1(a) can be addressed to some extent. However, response of battery to high frequency currents which affects battery life is the major limitation of the connection in Fig.1(b). On the other hand, effect of linear charging/discharging characteristics of supercapacitor on dc-link voltage, less volumetric efficiency and requirement of large capacity supercapacitor are the limitations of the configuration in Fig. 1(c).

The series and parallel connected fully active configurations are shown in Fig. 1(d) and Fig. 1(e) respectively. In these configurations, both battery and supercapacitor have been interfaced via dc-dc converters. Hence, problems of volumetric efficiency and control can be addressed with these configurations. However, wide operating voltage range of supercapacitor, poor transient power sharing among battery and supercapacitor and more ripple current at battery are the main drawbacks of these configurations. The active parallel configuration shown in Fig. 1(f), can address the issues with the above mentioned configurations at a cost of dedicated converters and complex control.



Mostly, in microgrid applications, configuration shown in Fig. 1(f) has been preferred. The typical microgrid configuration is shown in Fig. 2. considered the similar configuration shown in Fig. 2. Excellent system performance, effective power sharing and higher capacity utilization of supercapacitor is achieved. However, dedicated converters leads to high system cost, more power loss, control complexity, requirement of more number of sensors and less reliable. Moreover, since, supercapacitor has to respond only during sudden disturbances the supercapacitor converter remains ideal most of the time. Therefore, a multi-source converter based new system configuration for interfacing PV, wind ,battery and supercapacitor is proposed which can address the issues with above mentioned configurations without having a dedicated converters and complex control. The proposed configuration is well suited for dc microgrid applications. The key contri- butions of the proposed system are

- i. Interfacing of multiple sources with less number of components.
- ii. Inherent voltage boosting.
- iii. Inherent voltage regulation of supercapacitor.
- iv. Power sharing among battery and supercapacitor is inherently achieved.
- v. Controller is simple with less number of sensors and designed to maintain power balance in the system along with Maximum Power Point (MPP) operation of PV and wind.

The organization of the paper is as follows; Section II discusses the system configuration, operational modes and design aspects. Section III discusses the control structure, small signal modeling and stability analysis. Section IV and V discusses the simulation and experimental results. Section VI discusses the key conclusions followed by references

## II.PROPOSED MULTI-SOURCE CONVERTER CONFIGURATION

The proposed system configuration is shown in Fig. 3. PV and HES are interfaced using bi-directional buck-boost dc-dc converter and wind is interfaced to dc-link using dc-dc boost converter.  $L_{ph}$ ,  $L_w$  and  $L_b$  are the inductance of Photovoltaic Hybrid Converter (PHC), wind converter and HES decoupling inductor respectively.  $V_{pv}$ ,  $V_b$ ,  $V_{sc}$ ,  $V_{hes}$ ,  $V_w$  and  $V_{dc}$  are the voltages of PV, battery, supercapacitor, HES wind and dc-link voltages respectively.  $i_{pv}$ ,  $i_{ph}$ ,  $i_b$ ,  $i_{sc}$ ,  $i_w$ ,  $i_{dc}$  are PV,  $L_{ph}$ , battery, supercapacitor, wind and dc-link currents respectively.  $R_{dc}$ ,  $r_b$  and  $r_{sc}$  are load resistance, internal resistance of battery and supercapacitor respectively.  $S_1$ ,  $S_2$  are switches of PHC and  $D_3$ ,  $S_4$  are the switches of wind converter.  $D_{ph}$  and  $D_w$  are the duty cycles of PHC and wind converter respectively.

When PV is available, charging/discharging of battery and MPP operation of PV is achieved by operating the switches  $S_1$  and  $S_2$ . When PV is absent, the voltage across  $C_{pv}$  is main- tained by HES such that voltage at dc-link should be regulated at reference voltage ( $v_{dcr}$ ) by operating the switches  $S_1$  and  $S_2$ . Similarly, switches  $D_3$  and  $S_4$  are controlled to achieve MPP operation of wind. The HES takes the excess/deficit power at dc-link in-which battery takes average power and supercapacitor takes oscillatory power. The current decoupling frequency between battery and supercapacitor depends on  $L_b$ ,  $C_{sc}$ ,  $r_{sc}$ ,  $r_b$ . When  $S_1$  is on, operational and electrical equivalent circuits are shown in Fig. 4(a), Fig. 4(b). In this mode

$$V_{ph} = V_{pv}; V_{dc} = V_{pv} + V_{hes}$$

When  $S_2$  is on, operational and electrical equivalent circuits are shown in Fig. 4(c), Fig. 4(d). In this mode

$$V_{ph} = V_{hes}; V_{dc} = V_{pv} + V_{hes}$$

Therefore, in both the modes dc-link voltage is the sum of PV and HES voltages which shows the inherent boosting capability of the proposed configuration. Similarly, when  $D_3$ ,  $S_4$  is ON operational and electrical equivalent circuits are shown in Fig. 4(e), Fig. 4(f), Fig. 4(g), Fig. 4(h) and the steady state dc-link voltage can be expressed as

$$v_{dc} = \frac{v_w}{1 - D_w}$$

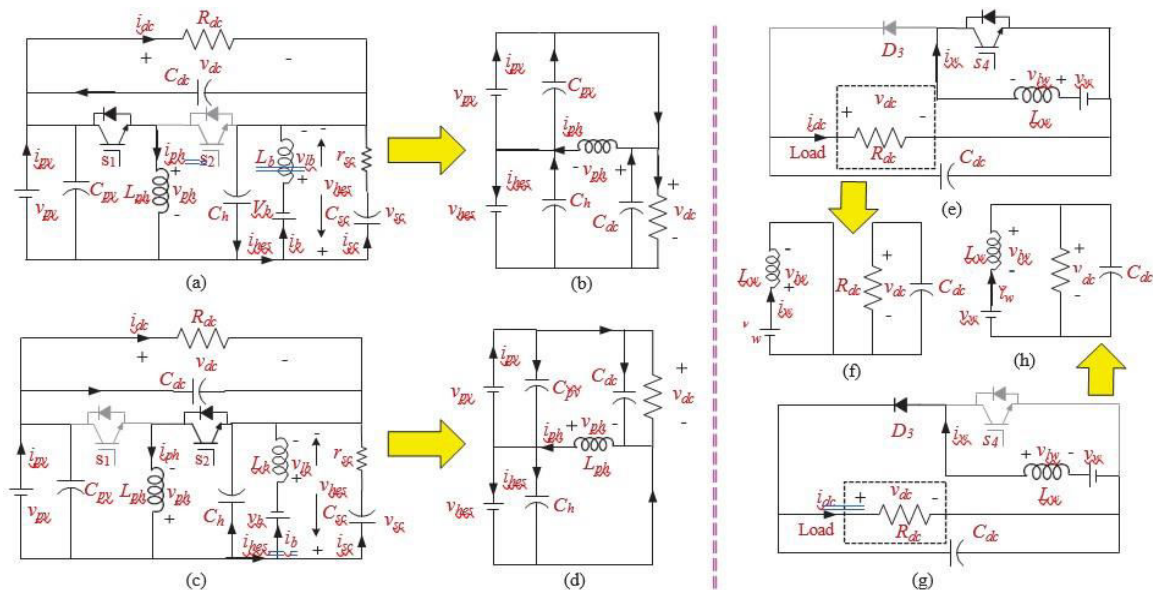


FIG 4: (a) Operating mode when  $S_1$  of PHC is ON. (b) Equivalent circuit of PHC when  $S_1$  is ON. (c) Operating mode when  $S_2$  of PHC is ON. (d) Equivalent circuit of PHC when  $S_2$  is ON. (e) Operating mode when  $S_3$  of wind converter is ON. (f) Equivalent circuit of wind converter when  $S_4$  is ON. (g) Operating mode when  $D_3$  of wind converter is ON. (h) Equivalent circuit of wind converter when  $D_3$  is ON.

Under steady state,

$$I_{ph} = I_{hes} + I_{pv}$$

Hence by controlling the inductor current ( $i_{ph}$ ) both  $i_{pv}$  and  $i_{hes}$  can be controlled. The steady state operational waveforms based on control of switches is shown in Fig.5. When switches  $S_1, S_4$  are ON and  $S_2$  is OFF, the inductors  $L_{ph}$  and  $L_w$  charges with a current slope of  $v_{ph}/L_{ph}$  and  $v_w/L_w$  respectively. Capacitor  $C_h$  discharges through HES and load is being supplied by  $C_{dc}$  during this interval. Similarly, when  $S_1, S_4$  are OFF and  $S_2$  is ON, the inductors  $L_{ph}$  and  $L_w$  discharges through HES and load respectively. During this interval PV supplies load and  $C_{dc}$  through  $L_{ph}$ .

### A. System Design Considerations

The equivalent circuit of HES unit is shown in Fig. 6. By applying the Norton theorem, the ratio of battery current  $i_b$  and HES current ( $i_{hes}$ ) in s-domain

Hence, the behavior of HES can be analyzed with the help of transfer function  $G_{ibh}(s)$  and current decoupling frequency can be written as

$$= \frac{(r_b + r_{sc})C_{sc} - \sqrt{(r_b + r_{sc})^2 C_{sc}^2 - 4 L_b C_{sc}}}{4\pi L_b C_{sc} f_c}$$

The values  $r_b$  and  $r_{sc}$  are taken from the data-sheets of battery and supercapacitor respectively. The decoupling frequency can be determined based on the safer di/dt limits of battery. The bode plot of  $G_{ibh}(s)$  for different values of  $L_b$  is shown in Fig.7. The minimum value of  $L_b$  is chosen such that the magnitude (db) of current  $i_b$  is well less-than -20db at higher frequencies. Therefore, with the selected values of  $L_b$  and  $f_c$  the value of capacitance  $C_{sc}$  is chosen. Since, dc-link voltage  $V_{dc}$  depends on  $V_{pv}$  and  $V_{hes}$ , the values of  $V_{pv}$  and  $V_{hes}$  is chosen such that dc-link voltage is maintained at minimum desired value even at worst conditions such as minimum State of Charge (SoC) of battery and minimum irradiance levels of PV. The transfer function of battery and supercapacitor voltages can be written from Fig. 5 as follows

$$G_{vbsc}(s) = v_{sc} = \frac{v_{sc} s^2 + s r_{sc} C_{sc} + r_{sc} C_{sc}}{s^2 L_b C_{sc} + s C_{sc} + 1}$$

Under steady state, the battery voltage is equal to the super- capacitor voltage. Hence, the voltage rating of supercapacitor is chosen to be bit higher than battery voltage so that inherent voltage regulation of supercapacitor can be achieved. Apart from the considerable advantages of the proposed configura- tion, the limitation of the proposed configura- tion is that dc- link voltage cannot be tightly regulated when PV is present. However, the voltage variation is with-in the permissible range. The PHC converter is having a synchronous switch which ensures CCM operation during all the load conditions by allowing negative current in the inductor. Hence, the problem of DCM can be avoided in the PHC converter. The output voltage of the wind converter, nothing but voltage  $v_{dc}$  which is always maintained at a specific value by the PV and HES. Hence by selecting the value of inductor to operate the converter in CCM at minimum value of duty cycle, DCM can be avoided *in the PHC converter*

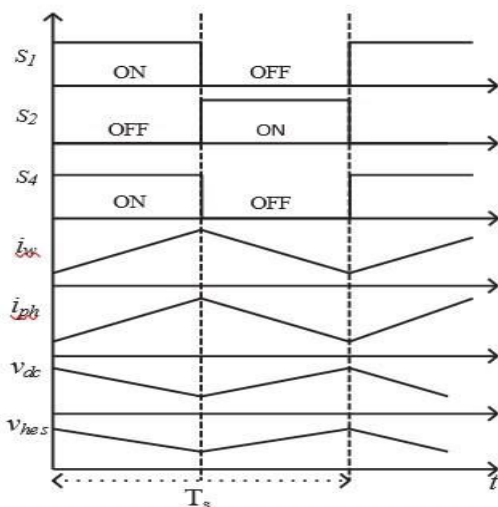


Fig. 5. Steady state operational waveforms

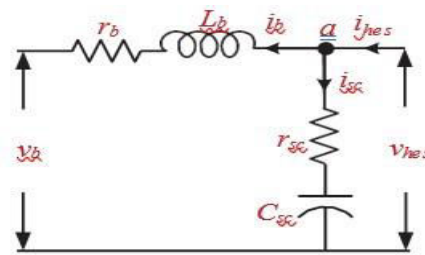


Fig. 6. Equivalent circuit of HES unit with

current based on control of switches

sharing among battery and supercapacitor

### III.SIMULATION DIAGRAM

#### MAIN CIRCUIT:

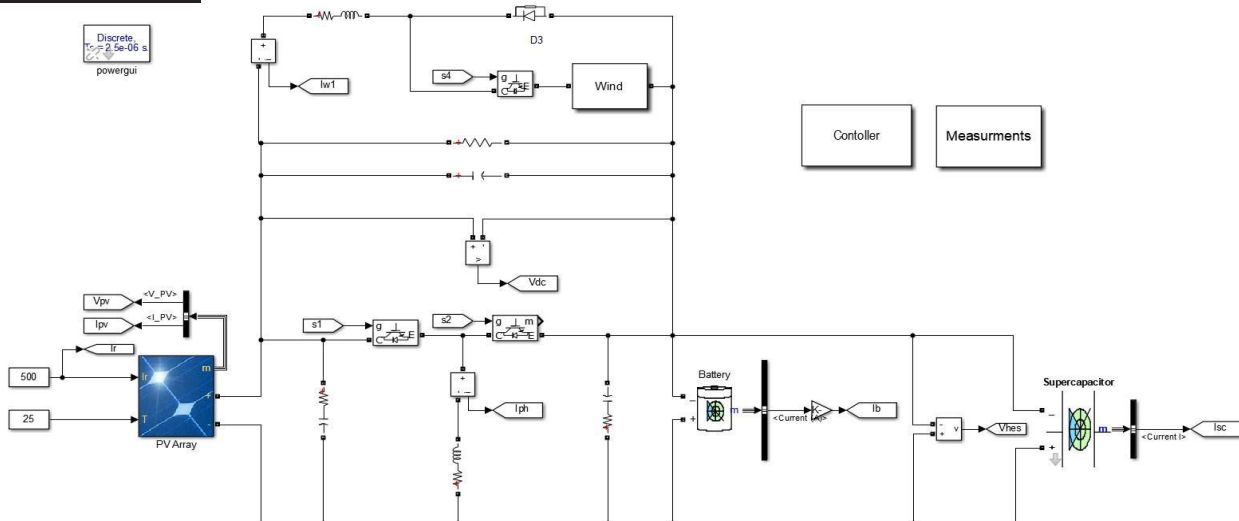


Fig.7. simulation diagram of p-v, wind and HES multi source converter

The MPP current generated by the wind MPP algorithm is the reference current for wind controller. The actual wind current ( $i_w$ ) and the reference current ( $i_{wr}$ ) is compared and the error is fed to Proportional-Integral (PI) current controller. PI controller generates required duty cycle to make error zero. In-order to generate switching pulses, generated duty cycle ( $d_w$ ) is compared with high frequency ramp signal which decides the switching frequency of the converter.

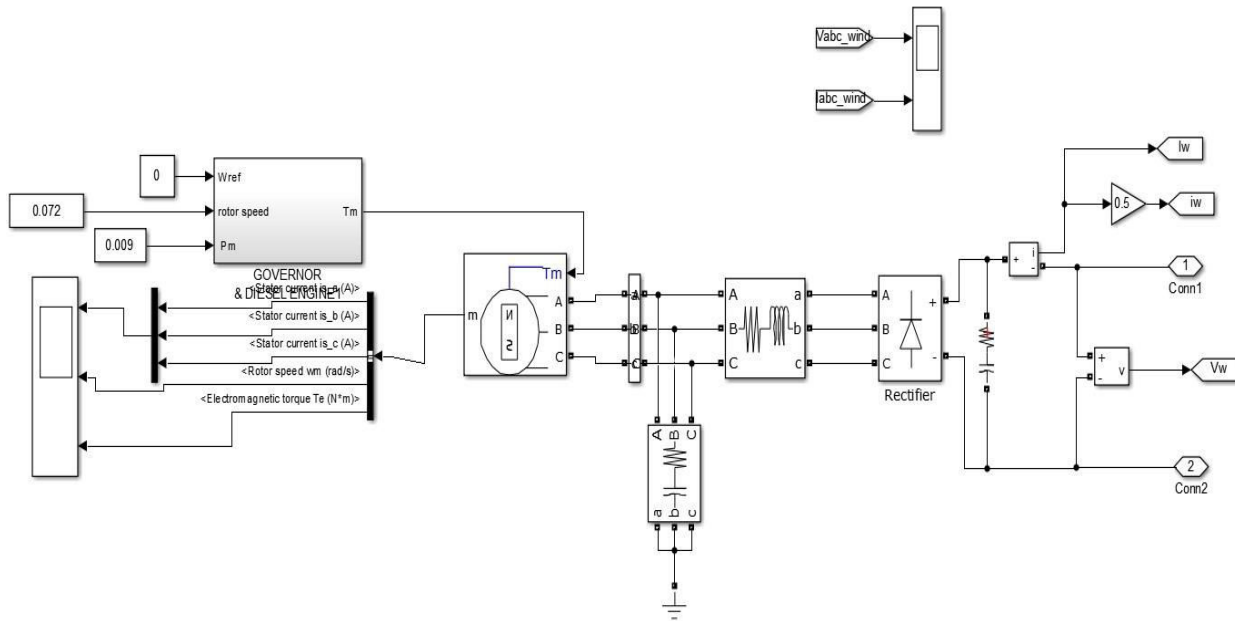


Fig.8. simulation diagram of wind energy

The experimental results are shown to evaluate the system performance under load and source changes during different operating conditions. Battery, super- capacitor PV, wind and inductor current sensors are connected in such a way that negative polarity of battery/supercapacitor currents indicate discharging of battery/supercapacitor, negative polarity of PV current indicates supplying of PV power and positive polarity of wind current indicates supplying of wind power.

TABLE I  
SYSTEM PARAMETERS FOR SIMULATION AND EXPERIMENTAL STUDY

Parameters	Values
<b>Photovoltaic Source Parameters</b>	
Voltage at MPP ( $V_{pv\_mpp}$ )	17.02 V
Current at MPP ( $i_{pv\_mpp}$ )	2.8 A
<b>Battery pack:</b>	
Terminal voltage ( $V_b$ )	36 V
Capacity	32 Ah
<b>Supercapacitor pack</b>	
Terminal Voltage ( $V_{sc}$ )	40 V
Capacitance ( $C_{sc}$ )	9.6 F
<b>Wind Source Parameters</b>	
Voltage at MPP ( $V_{w\_mpp}$ )	30 V
Current at MPP ( $i_{w\_mpp}$ )	3 A
<b>Converter Parameters</b>	
	$L_{cb} = 2 \text{ mH}$ , $L_{cb} = 5 \text{ mH}$ , $L_w = 2 \text{ mH}$ , $C_{pv} = 2200 \text{ }\mu\text{F}$ , $C_h = 2200 \text{ }\mu\text{F}$ , $C_w = 1000 \text{ }\mu\text{F}$
<b>Load Parameters</b>	
	$R_{dc} = (10 - 100) \text{ }\Omega$



IV.SIMULATION RESULTS AND DISCUSSIONS

MATLAB/Simulink is used as a platform to carry out digital simulations in order to evaluate the proposed system performance under different operating conditions. Table I shows the system parameters used for simulation studies. Solar irradiance, wind MPP current and load resistance is varied intentionally to verify the efficacy of proposed control structure. The performance of proposed system is verified under basic operating conditions such as (i) PV and Wind power is available (ii) Only wind power is available (iii) Only PV power is available and (iv) Both PV and wind is OFF.

A. Both PV and wind power are off

This operating condition is shown in Fig. 9. Since both PV and wind are OFF the total load power is solely supplied by storage unit. Therefore, from Fig. 9 it can be observed that during all the disturbances transient/oscillatory power is supplied by the supercapacitor and the average/steady state power is supplied by battery.

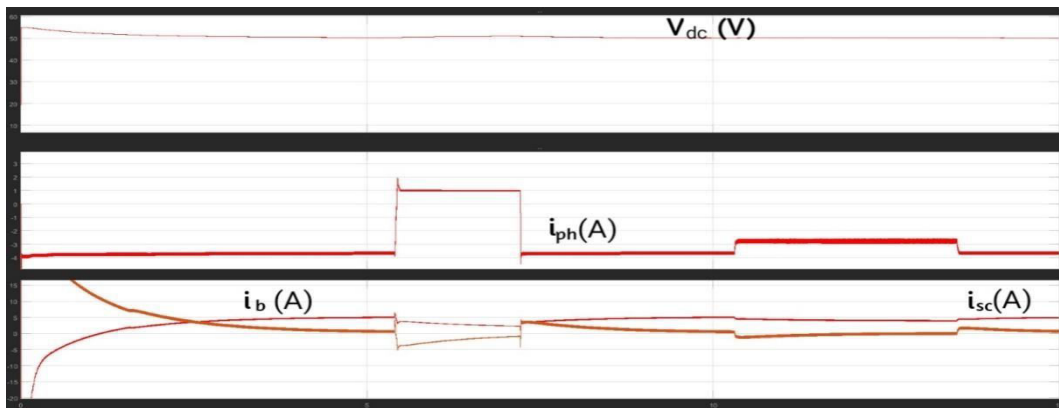


Fig. 9. Simulation results showing the system performance during the operating condition when PV and wind are OFF.

B. Only PV power is available

This condition is shown in Fig. 10. During this operating condition PV and load disturbances are created at regular intervals of time. At  $t = 8s$  and  $t = 16s$  solar irradiance is decreased from 1000 to 600 and 100  $W/m^2$  respectively. Similarly load disturbances are created at  $t = 24s$  and  $t = 28s$ . In this mode, the dc-link voltage varies when PV irradiance is changing over time which can be observed for Fig. 10. The dc-link voltage variations are quantified and presented in Table II.

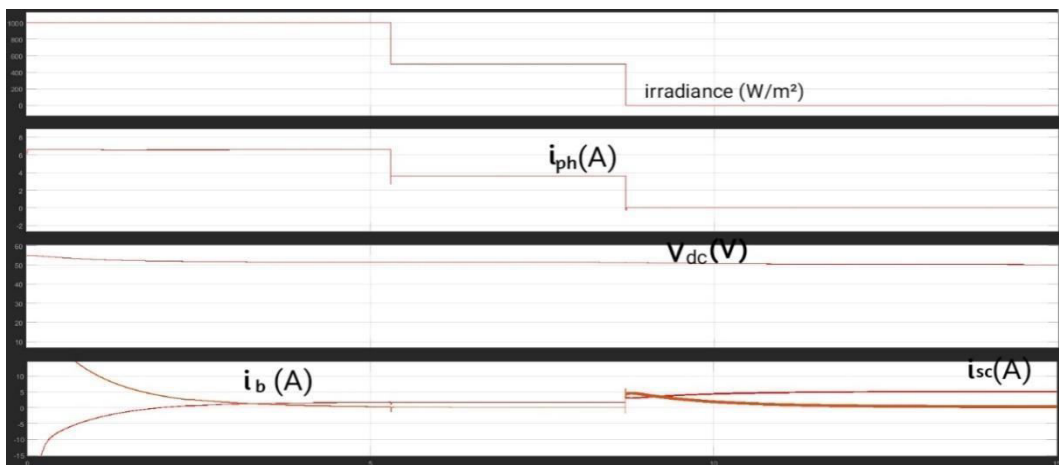


Fig. 10. Simulation results showing the system performance during the operating condition when PV power is available.



**C. Only wind power is available**

This operating condition is shown in Fig. 11. In this mode, load is being supplied by wind and storage unit. Wind disturbances are created at  $t = 8s$ ,  $t = 24s$  and load disturbances are created at  $t = 6s$ ,  $t = 28s$ . From Fig. 11 it can be observed that dc-link voltage is regulated. Moreover, transient power is being supplied by supercapacitor and average power by battery.

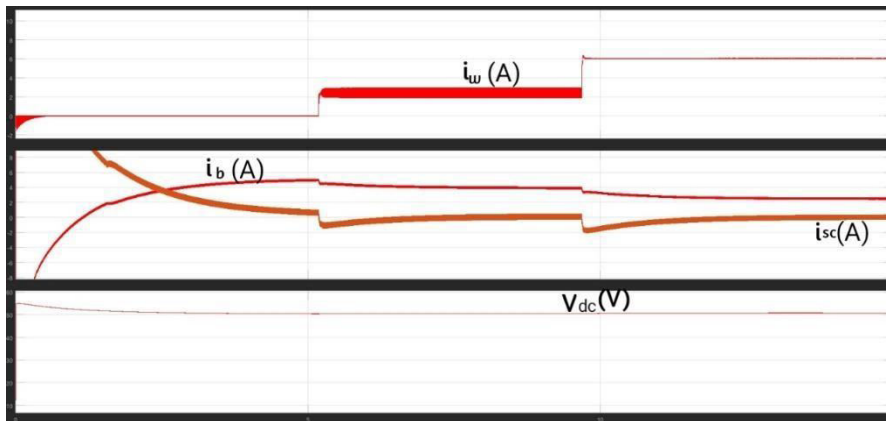


Fig.11 Simulation results showing the system performance during the operating condition when wind power is available

**D. Both PV and wind power are available**

The performance of the system during this operating condition is shown in Fig. 12. During this operating condition PV, wind and load disturbances are created at regular intervals of time. At  $t = 8s$ , PV disturbance is created. At  $t = 16s$ , wind disturbance is created. Similarly, load disturbance is created at  $t = 24s$ . From Fig. 12, it is observed that power balance is maintained in the system during all the disturbances.

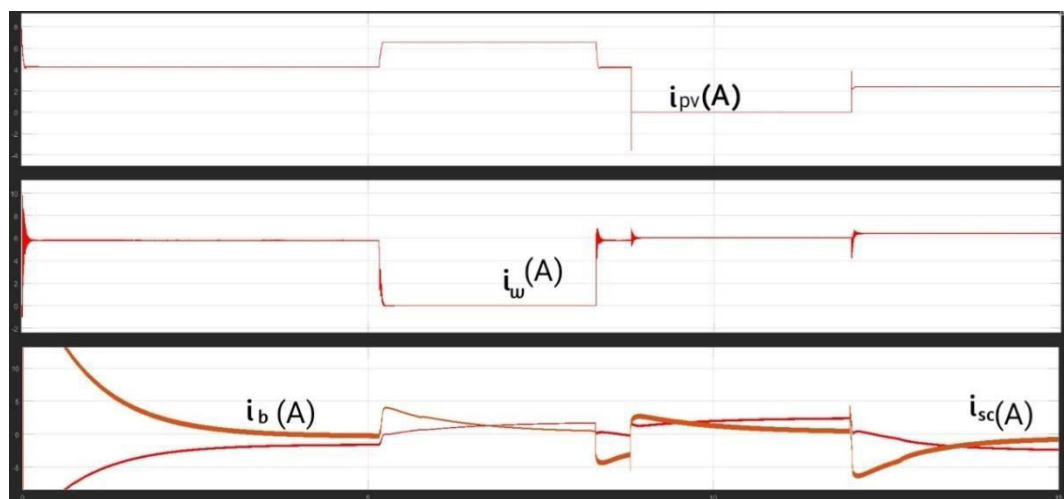


Fig.12 Simulation results showing the system performance during the operating condition when PV and wind power are available.

**VI.CONCLUSION**

A new multi-source converter configuration to interface PV, wind and battery-supercapacitor based Hybrid Energy Storage for DC microgrid applications along with detailed analysis, modeling and control structure design was presented. The efficacy of proposed configuration and control was verified through simulation results under various cases such as (i) Both PV and wind power is available (ii) Only wind power is available (iii) Only PV power is



available and (iv) Both PV and wind is OFF. The satisfactory performance was observed along with basic functionality such as operating renewable sources (PV and wind) at Maximum Power Point and charging and discharging of energy storage based on availability of power

## REFERENCES

1. H. M. Al-Masri and M. Ehsani, "Feasibility investigation of a hybrid on-grid wind photovoltaic retrofitting system," *IEEE Trans. Ind. Appl.*, vol. 52, DOI 10.1109/TIA.2015.2513385, no. 3, pp. 1979–1988, May.2016.
2. S. Kotra and M. K. Mishra, "A supervisory power management system for a hybrid microgrid with hess," *IEEE Trans. Ind. Electron.*, vol. 64, DOI 10.1109/TIE.2017.2652345, no. 5, pp. 3640–3649, May. 2017.
3. C. Abbey and G. Joos, "Supercapacitor energy storage for wind energy applications," *IEEE Trans. Ind. Appl.*, vol. 43, DOI 10.1109/TIA.2007.895768, no. 3, pp. 769–776, May. 2007.
4. R. A. Dougal, S. Liu, and R. E. White, "Power and life extension of battery-ultracapacitor hybrids," *IEEE Trans. Comp. and Packaging Tech.*, vol. 25, DOI 10.1109/6144.991184, no. 1, pp. 120–131, Mar. 2002.
5. S. Adhikari, Zhang Lei, Wang Peng, and Yi Tang, "A battery/supercapacitor hybrid energy storage system for dc micro-grids," in *Proc. IEEE 8th Int. Power Electron and Motion Control Conf.(IPEMCECCE Asia)*, DOI 10.1109/IPEMC.2016.7512558, pp. 1747–1753, May. 2016.
6. Z. Song, J. Hou, H. F. Hofmann, X. Lin, and J. Sun, "Parameter identification and maximum power estimation of battery/supercapacitor hybrid energy storage system based on cramerârao bound analysis," *IEEE Trans. Power Electron.*, vol. 34, DOI 10.1109/TPEL.2018.2859317, no. 5, pp. 4831–4843, May. 2019.
7. Khaligh and Z. Li, "Battery, ultracapacitor, fuel cell, and hybrid energy storage systems for electric, hybrid electric, fuel cell, and plug-in hybrid electric vehicles: State of the art," *IEEE Trans. on Vehicular Tech.*, vol. 59, DOI 10.1109/TVT.2010.2047877, no. 6, pp. 2806–2814, Jul. 2010.
8. W. Jing, C. Hung Lai, S. H. W. Wong, and M. L. D. Wong, "Battery-supercapacitor hybrid energy storage system in standalone dc micro-grids: a review," *IET Renewable Power Gen.*, vol. 11, DOI 10.1049/iet-rpg.2016.0500, no. 4, pp. 461–469, 2017.
9. T. Kamal, M. Karabacak, S. Z. Hassan, H. Li, A. Arsalan, and R. K. Rajkumar, "Integration and control of an offgrid hybrid wind/pv generation system for rural applications," in *in Proc. IEEE Intern. Conf. on Innovations in Elect. Eng. and Computational Tech. (ICIEECT)*, DOI 10.1109/ICIEECT.2017.7916543, pp. 1–6, Apr. 2017.
10. S. K. Kollimalla, M. K. Mishra, A. Ukil, and H. B. Gooi, "Dc grid voltage regulation using new hess control strategy," *IEEE Trans. on Sustain. Energy*, vol. 8, DOI 10.1109/TSTE.2016.2619759, no. 2, pp. 772–781, Apr. 2017.
11. S. K. Kollimalla, A. Ukil, H. B. Gooi, U. Manandhar, and N. R. Tummuru, "Optimization of charge/discharge rates of a battery using a two-stage rate-limit control," *IEEE Trans. on Sustain. Energy*, vol. 8, DOI 10.1109/TSTE.2016.2608968, no. 2, pp. 516–529, Apr. 2017.
12. S. K. Kollimalla, M. K. Mishra, and N. L. Narasamma, "Design and analysis of novel control strategy for battery and supercapacitor storage system," *IEEE Trans. on Sustain. Energy*, vol. 5, DOI 10.1109/TSTE.2014.2336896, no. 4, pp. 1137–1144, Oct. 2014.
13. U. Manandhar, N. R. Tummuru, S. K. Kollimalla, A. Ukil, G. H. Beng, and K. Chaudhari, "Validation of faster joint control strategy for battery- and supercapacitor-based energy storage system," *IEEE Trans. Ind. Electron.*, vol. 65, DOI 10.1109/TIE.2017.2750622, no. 4, pp. 3286–3295, Apr. 2018.
14. N. R. Tummuru, M. K. Mishra, and S. Srinivas, "Dynamic energy management of hybrid energy storage system with high-gain pv converter," *IEEE Trans. Energy Convers.*, vol. 30, DOI 10.1109/TEC.2014.2357076, no. 1, pp. 150–160, Mar. 2015.
15. Q. Xu, J. Xiao, P. Wang, X. Pan, and C. Wen, "A decentralized control strategy for autonomous transient power sharing and state-of-charge recovery in hybrid energy storage systems," *IEEE Trans. on Sustain. Energy*, vol. 8, DOI 10.1109/TSTE.2017.2688391, no. 4, pp. 1443–1452, Oct. 2017.
16. Tani, M. B. Camara, and B. Dakyo, "Energy management in the decentralized generation systems based on renewable energy ultracapacitors and battery to compensate the wind/load power fluctuations," *IEEE Trans. Ind. Appl.*, vol. 51, DOI 10.1109/TIA.2014.2354737, no. 2, pp. 1817–1827, Mar. 2015.



**INNO SPACE**  
SJIF Scientific Journal Impact Factor  
**Impact Factor: 8.423**



**ISSN** INTERNATIONAL  
STANDARD  
SERIAL  
NUMBER  
INDIA



# INTERNATIONAL JOURNAL OF INNOVATIVE RESEARCH

IN SCIENCE | ENGINEERING | TECHNOLOGY

**9940 572 462** **6381 907 438** **ijirset@gmail.com**



[www.ijirset.com](http://www.ijirset.com)

Scan to save the contact details